EUROPEAN JOURNAL OF PURE AND APPLIED MATHEMATICS
2026, Vol. 19, Issue 1, Article Number 7155
ISSN 1307-5543 – ejpam.com
Published by New York Business Global

Numerical Study of Time–Fractional Cattaneo Equation via the Atangana–Baleanu–Caputo Operator

Kamel Al-Khaled[1], Abdullah Alsoboh[2], Ahmad Al Kasbi[2,*], Mahmood Shareef Ajeel[3], Shreen Tamimi[1], Hala K. Al-Khalid[4]

[1] *Department of Mathematics and Statistics, Jordan University of Science and Technology, Irbid 22110, Jordan*
[2] *College of Applied and Health Sciences, A'Sharqiyah, P.O. Box 42, Post Code 400, Ibra, Sultanate of Oman*
[3] *Department of Material Engineering, College of Engineering, Shatrah University, Thi-Qar 64001, Iraq*
[4] *Department of Mathematics, Western Michigan University, Kalamazoo, MI 49008-5248, USA*

Abstract. Fractional models play a vital role in describing diffusion and heat transfer processes characterized by memory and nonlocal effects. In this work, a novel spectral collocation method is developed for solving the time–fractional Cattaneo equation involving the Atangana–Baleanu–Caputo (ABC) fractional derivative. The proposed approach employs two-dimensional expansions of shifted Legendre polynomials over the space–time domain, thereby transforming the fractional problem into a system of algebraic equations. The novelty of this study lies in employing the ABC fractional operator with a generalized Mittag–Leffler kernel within a Legendre spectral–collocation framework, providing improved accuracy and stability compared with existing approaches. Comprehensive numerical experiments confirm that the proposed Legendre spectral scheme exhibits excellent agreement with analytical solutions and reduces the approximation error by approximately 50% compared with previously reported spline-based techniques. The obtained results demonstrate that the developed approach is a reliable, accurate, and efficient tool for modeling diffusion processes governed by fractional Cattaneo dynamics.

2020 Mathematics Subject Classifications: 65M70, 26A33, 35R11, 92C45

Key Words and Phrases: Time-fractional Cattaneo equation, Atangana–Baleanu–Caputo (ABC) fractional derivative, two-dimensional shifted Legendre polynomials, spectral method.

*Corresponding author.
DOI: https://doi.org/10.29020/nybg.ejpam.v19i1.7155

Email addresses: kamel@just.edu.jo (K. Al-Khaled), abdullah.alsoboh@asu.edu.om (A. Alsoboh), ahmed.alkasbi@asu.edu.om (A. Al Kasbi), mahmoodshareef@shu.edu.iq (M. S. Ajeel), shreentamimi25@gmail.com (S. Tamimi), halakamelmustafa.alkhalid@wmich.edu (H. K. Al-Khalid)

List of Symbols and Abbreviations

For clarity and ease of reference, the main symbols, abbreviations, and parameters used throughout the manuscript are summarized in the following table.

Symbol	Description
$P_i(x), P_j(t)$	Shifted Legendre polynomials in space and time
$g_1(t), g_2(t)$	Boundary functions
$h(x,t)$	Source term
${}_0^{ABC}\mathrm{D}_t^{\alpha}$	Atangana–Baleanu–Caputo fractional derivative
$E_{\alpha,\mu}^{\gamma}(\cdot)$	Generalized Mittag–Leffler function
$q(x)$	Initial heat flux distribution
α	Fractional order ($1 < \alpha < 2$)
μ, γ	Kernel parameters of the ABC derivative
m, n	Polynomial degrees in spatial and temporal directions

1. Introduction

Fractional differential equations (FDEs) have emerged as powerful tools for modeling physical phenomena characterized by memory and hereditary effects. Unlike classical integer-order formulations, fractional models capture both local and global memory behaviors, providing more accurate descriptions of real-world systems [1]. A prominent example is the time-fractional Cattaneo equation, which extends Fourier's classical heat-conduction law by incorporating a fractional time derivative. This extension accounts for finite propagation speeds and memory effects, making the model particularly suitable for heat transport in materials with nonlocal responses [2].

Fractional calculus itself has become a versatile mathematical framework for describing anomalous dynamics across physics, engineering, biology, and finance. Several definitions of fractional derivatives have been proposed, including those of Riemann–Liouville, Caputo, Grünwald–Letnikov, and Hadamard, each with specific advantages and limitations related to initial conditions, kernel singularities, and physical applicability [1]. In 2016, Atangana and Baleanu introduced a new operator—now widely known as the Atangana–Baleanu–Caputo (ABC) derivative—based on a non-singular, non-local Mittag–Leffler kernel [3]. Unlike classical power-law kernels, the ABC derivative avoids singularities while preserving smoothness, non-local memory, and interpolation between integer- and fractional-order dynamics. These properties make the ABC derivative especially attractive for modeling complex dynamical systems with fading memory [4].

Classical Fourier theory assumes an infinite speed of thermal propagation, which is unrealistic in nanoscale, biological, and high-frequency thermal processes. The Cattaneo–Vernotte modification addressed this limitation by introducing a relaxation time, leading to hyperbolic heat conduction and finite-speed thermal waves. Nevertheless, such models remain inadequate for biological tissues, porous media, and nanostructures, where anomalous and memory-driven heat conduction dominates [2]. To overcome these challenges, researchers

have incorporated fractional operators into the Cattaneo framework. In one study, Algahtani et al. compared the Caputo–Fabrizio and Atangana–Baleanu formulations for a fractional Allen–Cahn reaction–diffusion model, highlighting the impact of kernel choice on the solution behavior. The ABC derivative, in particular, has been analyzed in the context of diffusion equations and shown to preserve stability while offering a more realistic memory effect due to the long-tail decay of the Mittag–Leffler kernel. These findings suggest that employing the ABC operator in fractional heat or diffusion equations, such as the Cattaneo model, can enhance the model's physical fidelity [5]. In particular, the ABC derivative—with its non-singular Mittag–Leffler kernel—overcomes key drawbacks of the Caputo and Riemann–Liouville operators, ensuring both thermodynamic consistency and strong memory retention.

The time-fractional Cattaneo equation has been successfully applied in several physical and engineering contexts. It models non-Fourier heat conduction in nanoscale materials, bioheat transfer in living tissues, and transient heat transport in porous and composite media. In energy systems, it describes phase-change thermal storage and thermal relaxation in solar collectors. These applications highlight the capability of fractional Cattaneo dynamics to capture finite-speed thermal propagation and long-memory effects more accurately than classical diffusion models[6, 7].

The time-fractional Cattaneo equation with the ABC derivative has broad relevance across disciplines. In biomedical engineering, it models laser-induced heating in tissues, where both finite propagation speed and memory effects are crucial. In materials science, it captures subdiffusive and ballistic heat conduction in composite and nanoscale structures. In geophysics, it describes slow heat transfer in geothermal reservoirs and stratified rock formations. In energy systems, it helps simulate thermal storage units employing phase-change materials (PCMs) with delayed thermal responses. These applications highlight the importance of developing efficient and accurate solution methods for this equation.

Several numerical approaches have been proposed for fractional Cattaneo models. For Caputo derivatives, fully discrete schemes combining Galerkin finite elements in space with convolution quadrature in time have been developed [8], supported by rigorous error estimates. Extensions with higher-order quadrature were presented [9]. For the Caputo–Fabrizio derivative, spline-based schemes—including cubic, trigonometric, and extended cubic B-splines—were introduced [10], with stability and error analysis ensuring reliability. While effective, these schemes are primarily numerical and may lack analytic interpretability, leaving room for methods that combine accuracy with analytical structure.

We study the ABC time-fractional Cattaneo equation on $0 \le x \le 1$, $t > 0$ [2]:

$$\frac{\partial}{\partial t} y(x,t) + {}_0^{ABC}\mathrm{D}_t^{\alpha} y(x,t) = \frac{\partial^2}{\partial x^2} y(x,t) + h(x,t), \quad 1 < \alpha < 2,\ \mu > 0,\ \gamma \in \mathbb{N}, \tag{1}$$

subject to the initial conditions

$$y(x,0) = h(x) \quad \text{and} \quad y_t(x,0) = q(x), \quad 0 \le x \le 1, \tag{2}$$

and the boundary conditions

$$y(0,t) = g_1(t) \quad \text{and} \quad y(1,t) = g_2(t), \quad t > 0, \tag{3}$$

where ${}_0^{ABC}\mathrm{D}_t^{\alpha}$ denotes the Atangana–Baleanu–Caputo fractional derivative with a nonsingular Mittag–Leffler kernel (defined in Section 2). Our goal is to construct a spectrally accurate, analytically interpretable discretization using a two-dimensional shifted-Legendre basis in both space and time.

Recently, spectral methods have gained considerable attention for fractional equations due to their high accuracy and efficiency. Li et al. developed a space–time spectral method for the one-dimensional time-fractional Cattaneo equation, achieving high-order accuracy in both time and space [11]. Kumar and Pandey applied a Legendre spectral method to nonlinear fractional reaction–diffusion equations with the Atangana–Baleanu derivative and reported superior accuracy compared with finite-difference approaches [12]. Likewise, orthonormal function techniques, such as wavelet-based schemes, have been used to solve fractional Cattaneo-type problems with excellent accuracy [13]. More recently, polynomial-based operational matrix methods—for example, those employing Chebyshev and Jacobi bases—have emerged as powerful tools for fractional PDEs, providing algebraic simplifications of fractional operators and enabling efficient computation [14, 15]. The authors addressed an inverse problem involving the simultaneous identification of the fractional order in a time-fractional Cattaneo equation [16]. Several studies [17–20] have applied Chebyshev and hybrid pseudospectral methods to fractional advection–diffusion and wave–diffusion problems, achieving high accuracy and numerical stability. Building on these advances, the present study extends the spectral-collocation framework to the (ABC) operator, incorporating a generalized Mittag–Leffler kernel to enhance convergence and capture non-singular memory effects.

Motivated by these developments, this paper proposes an analytical spectral-collocation method for solving the time-fractional Cattaneo equation involving the ABC fractional derivative. The solution $y(x,t)$ is approximated using a two-dimensional basis of shifted Legendre polynomials in both space and time, enabling a discretization that is highly accurate, efficient, and analytically interpretable. Comparative tests against existing results [2] demonstrate that the proposed approach reduces approximation error by more than half, confirming its robustness and effectiveness. The method can handle nonlinear fractional PDEs and other kernels with minor modifications [21, 22]. Recent studies on fractional epidemic and PDE models [23] highlight the growing role of advanced numerical methods, motivating this work.

The remainder of this paper is organized as follows. Section 2 presents the necessary preliminaries, including the definition of shifted Legendre polynomials and the ABC fractional derivative of the approximate solution. Section 3 introduces the proposed spectral-collocation method and its application to the time-fractional Cattaneo equation. Section 4 provides the convergence analysis, while Section 5 reports numerical experiments validating the accuracy and efficiency of the method. Finally, Section 6 concludes with a summary of the main results and potential directions for future research.

2. Mathematical Prelimaries

In this section, we present the one and two dimensions of the shifted Legendre polynomials with their properties and we define the Mittag-Leffler kernel. Also, we show the ABC fractional derivative and apply it on shifted Legendre polynomials.

Definition 1. *The recurrence formula for one dimension of shifted Legendre polynomials is defined on* $[0,1]$ *as follows [24]:*

$$\tilde{P}_{i+1}(x) = \frac{2i+1}{i+1}(2x-1)\tilde{P}_i(x) - \frac{i}{i+1}\tilde{P}_{i-1}(x), \quad i = 1, \ldots. \tag{4}$$

where $\tilde{P}_0(x) = 1$ *and* $\tilde{P}_1(x) = 2x-1$, *and the orthogonality relation is*

$$\int_0^1 \tilde{P}_i(x)\tilde{P}_j(x)dx = \begin{cases} \frac{1}{2j+1}, & i = j \\ 0 \quad , & i \neq j \end{cases} \tag{5}$$

The approximate solution defined for one dimension of shifted Legendre polynomials on $[0,1]$ *as follows*

$$y_m(x) = \sum_{i=0}^{m} c_i \tilde{P}_i(x), \tag{6}$$

where the coefficients of c_i *are given by*

$$c_i = (2i+1)\int_0^1 y_m(x)\tilde{P}_i(x)dx, \quad i = 0, 1, \ldots, m \tag{7}$$

where the one-dimensional shifted Legendre polynomials are orthogonal with respect to the weight function $w(x)$ *as:*

$$\int_0^1 w(x)\tilde{P}_m(x)\tilde{P}_n(x)dx = \begin{cases} \dfrac{1}{(2m+1)}, & \text{if} \quad m = n, \\ 0, & \text{otherwise.} \end{cases} \tag{8}$$

such that, the one dimension of shifted Legendre polynomials is:

$$\tilde{P}_i(x) = \sum_{k=0}^{i} \frac{(-1)^{i+k}(i+k)!}{(k!)^2(i-k)!}x^k, \tag{9}$$

Definition 2 (Approximate solution via shifted Legendre polynomials)**.** *The approximate solution* $y_{m,n}(x,t)$ *on* $[0,1]\times[0,1]$ *in terms of the two-dimensional shifted Legendre polynomials is given by [25]:*

$$y_{m,n}(x,t) = \sum_{i=0}^{m}\sum_{j=0}^{n} c_{ij}\,\tilde{P}_{i,j}(x,t) = \sum_{i=0}^{m}\sum_{j=0}^{n} c_{ij}\,\tilde{P}_i(x)\,\tilde{P}_j(t), \tag{10}$$

for $i = 0, \ldots, m$ and $j = 0, \ldots, n$. The coefficients c_{ij} are determined by

$$c_{ij} = (2i+1)(2j+1) \int_0^1 \int_0^1 y_{m,n}(x,t)\, \tilde{P}_i(x)\, \tilde{P}_j(t)\, dx\, dt, \qquad i = 0, \ldots, m,\ j = 0, \ldots, n. \tag{11}$$

The two-dimensional shifted Legendre polynomials are orthogonal with respect to the weight function $h(x,t)$ as follows [26]:

$$\int_0^1 \int_0^1 h(x,t)\, \tilde{P}_{ij}(x,t)\, \tilde{P}_{mn}(x,t)\, dx\, dt = \begin{cases} \dfrac{1}{(2i+1)(2j+1)}, & \text{if } i = m,\ j = n, \\ 0, & \text{otherwise.} \end{cases} \tag{12}$$

An explicit representation of the two-dimensional shifted Legendre polynomials is

$$\tilde{P}_{ij}(x,t) = \sum_{k=0}^{i} \sum_{h=0}^{j} \frac{(-1)^{\,i+j+k+h}\, (i+k)!\, (j+h)!}{(k!)^2\, (i-k)!\, (h!)^2\, (j-h)!}\, x^k\, t^h. \tag{13}$$

Definition 3. *Three types of Mittag-Leffler kernel is given by [27]:*

The Mittag-Leffler function of one parameter is

$$E_\alpha(\lambda, t) = \sum_{k=0}^{\infty} \lambda^k \frac{t^{\alpha k}}{\Gamma(\alpha k + 1)},\ \text{where } Re(\alpha) > 0,\ \lambda \in \mathbb{R} - \{0\}, \tag{14}$$

and the Mittag-Leffler function of two parameters is given by

$$E_{\alpha,\mu}(\lambda, t) = \sum_{k=0}^{\infty} \lambda^k \frac{t^{\alpha k + \mu - 1}}{\Gamma(\alpha k + \mu)},\ \text{where } Re(\alpha) > 0,\ \mu > 0 \text{ and } \lambda \in \mathbb{R} - \{0\}, \tag{15}$$

where the modified version of the Mittag- Leffler function of three parameters is

$$E^{\gamma}_{\alpha,\mu}(\lambda, t) = \sum_{k=0}^{\infty} \lambda^k \frac{(\gamma)_k\, t^{\alpha k + \mu - 1}}{\Gamma(\alpha k + \mu)},\ \text{where } Re(\alpha) > 0,\ \mu > 0,\ \gamma \in \mathbb{N} \text{ and } \lambda \in \mathbb{R} - \{0\}. \tag{16}$$

Definition 4. *The left generalized ABC fractional derivative with Mittag-Leffler kernel for $n < \alpha \leq n+1$, $\mu > 0$, $\lambda = -\frac{\alpha_1}{1-\alpha_1}$ and $\gamma \in N$ is defined as follows [28]:*

$${}^{ABC}_{0} D^{\alpha}_{x} f(x) = \frac{B(\alpha_1)}{1-\alpha_1} \int_0^x E^{\gamma}_{\alpha_1,\mu}(\lambda, x-t) f^{n+1}(t) dt, \tag{17}$$

where $E^{\gamma}_{\alpha_1,\mu}(\lambda, x-t)$ is defined in equation (16). Also, $B(\alpha_1) = 1$ is a normalization function and $\alpha_1 = \alpha - n$ with $n \in \mathrm{N}_0$.

The ABC fractional derivative for $n < \alpha \leq n+1$, $\mu > 0$ and $\gamma \in \mathbb{N}$ satisfies the following properties:

- $({}_0^{ABC}\mathrm{D}_x^{\alpha} c) = 0$ where c is constant.
- $({}_0^{ABC}\mathrm{D}_x^{\alpha} c * f)(x) = c * ({}_0^{ABC}\mathrm{D}_x^{\alpha} f)(x)$.
- $({}_0^{ABC}\mathrm{D}_x^{\alpha} f + g)(x) = ({}_0^{ABC}\mathrm{D}_x^{\alpha} f)(x) + ({}_0^{ABC}\mathrm{D}_x^{\alpha} g)(x)$.
- ${}_0^{ABC}\mathrm{D}_x^{\alpha} x^k = \frac{B(\alpha_1)}{1-\alpha_1}\Gamma(k+1)E^{\gamma}_{\alpha_1,\mu+k-n}(\lambda, x), \quad for \quad k > n, \quad n \in \mathrm{N}.$
- ${}_0^{ABC}\mathrm{D}_x^{\alpha} x^k = 0, for \quad k \leq n, \quad n \in \mathrm{N}.$

Theorem 1. *The left Atangana–Baleanu–Caputo (ABC) fractional derivative of the approximate solution expressed as a two-dimensional expansion of shifted Legendre polynomials, for $n < \alpha < n+1$, $\mu > 0$, $\alpha_1 = \alpha - n$, $\lambda = \frac{\alpha_1}{1-\alpha_1}$ and $\gamma \in N$, is given by:*

$$ {}_0^{ABC}D_t^{\alpha} y_{m,n}(x,t) = \sum_{i=0}^{m}\sum_{j=0}^{n} c_{ij}\tilde{P}_i(x)\sum_{k=0}^{j}\frac{(-1)^{j+k}(j+k)!}{(k!)^2(j-k)!}\frac{B(\alpha_1)}{1-\alpha_1}\Gamma(k+1)E^{\gamma}_{\alpha_1,\mu+k-n}(\lambda,t) \tag{18}$$

Proof.

$$ {}_0^{ABC}\mathrm{D}_t^{\alpha} y_{m,n}(x,t) = \sum_{i=0}^{m}\sum_{j=0}^{n} c_{ij}\tilde{P}_i(x)\,{}_0^{ABC}\mathrm{D}_t^{\alpha,\mu,\gamma}\tilde{P}_j(t) \tag{19}$$

$$ = \sum_{i=0}^{m}\sum_{j=0}^{n} c_{ij}\tilde{P}_i(x)\sum_{k=0}^{j}\frac{(-1)^{j+k}(j+k)!}{(k!)^2(j-k)!}\,{}_0^{ABC}\mathrm{D}_t^{\alpha,\mu,\gamma} t^k \tag{20}$$

$$ = \sum_{i=0}^{m}\sum_{j=0}^{n} c_{ij}\tilde{P}_i(x)\sum_{k=0}^{j}\frac{(-1)^{j+k}(j+k)!}{(k!)^2(j-k)!}\frac{B(\alpha_1)}{1-\alpha_1}\Gamma(k+1)E^{\gamma}_{\alpha_1,\mu+k-n} \tag{21}$$

3. Numerical Implementation

In this section, we present the proposed spectral method, which approximates the solution $y_{m,n}(x,t)$ using a two-dimensional expansion of shifted Legendre polynomials. We also demonstrate the corresponding one-dimensional case for completeness.

We introduce the vector for first $(m+1)$ of shifted Legendre polynomials as

$$\Phi(x) = \begin{bmatrix} \tilde{P}_0(x) \\ \tilde{P}_1(x) \\ \vdots \\ \tilde{P}_m(x) \end{bmatrix} \tag{22}$$

Accordingly, the approximate solution of the function $y_m(x)$ using shifted Legendre polynomials on $[0,1]$ can be expressed as:

$$y_m(x) = \sum_{i=0}^{m} c_i\tilde{P}_i(x) = C^T\,\Phi(x), \tag{23}$$

where

$$C = [c_0, c_1, \ldots, c_m]^T,$$

For the two-dimensional domain $(x,t) \in [0,1] \times [0,1]$, the approximate solution $y_{m,n}(x,t)$ is expressed as

$$y_{m,n}(x,t) = \sum_{i=0}^{m}\sum_{j=0}^{n} c_{ij}\tilde{P}_{i,j}(x,t) = \sum_{i=0}^{m}\sum_{j=0}^{n} c_{ij}\tilde{P}_i(x)\tilde{P}_j(t) = \Phi(x)^T C\ \Upsilon(t), \tag{24}$$

where

$$C = [c_{00}, c_{01}, \ldots, c_{0n}, \ldots, c_{m0}, c_{m1}, \ldots, c_{mn}], \quad \Phi(t) = [\tilde{P}_0(t), \tilde{P}_1(t), \ldots, \tilde{P}_n(t)]^T.$$

The vectors and coefficient matrix in Eq. (24) are defined with their precise dimensions as follows:

$$\Phi(x) = \begin{bmatrix} \tilde{P}_0(x) \\ \tilde{P}_1(x) \\ \vdots \\ \tilde{P}_m(x) \end{bmatrix} \in \mathbb{R}^{(m+1)\times 1}, \qquad \Upsilon(t) = \begin{bmatrix} \tilde{P}_0(t) \\ \tilde{P}_1(t) \\ \vdots \\ \tilde{P}_n(t) \end{bmatrix} \in \mathbb{R}^{(n+1)\times 1},$$

and the coefficient matrix

$$C = [c_{ij}]_{(m+1)\times(n+1)} \in \mathbb{R}^{(m+1)\times(n+1)}.$$

Thus, the term

$$y_{m,n}(x,t) = \Phi(x)^T C \Upsilon(t)$$

is dimensionally consistent, since $\Phi(x)^T \in \mathbb{R}^{1\times(m+1)}$, $C \in \mathbb{R}^{(m+1)\times(n+1)}$, and $\Upsilon(t) \in \mathbb{R}^{(n+1)\times 1}$, which results in a scalar value $y_{m,n}(x,t) \in \mathbb{R}$. This clarification ensures the proper two-dimensional structure of the approximation. Also,

$$\Upsilon(t) = \begin{bmatrix} \sum_{k=0}^{0} \frac{(-1)^{i+k}(i+k)!}{(k!)^2(i-k)!} t^k \\ \sum_{k=0}^{1} \frac{(-1)^{i+k}(i+k)!}{(k!)^2(i-k)!} t^k \\ \sum_{k=0}^{2} \frac{(-1)^{i+k}(i+k)!}{(k!)^2(i-k)!} t^k \\ \vdots \\ \sum_{k=0}^{m} \frac{(-1)^{i+k}(i+k)!}{(k!)^2(i-k)!} t^k \end{bmatrix} \tag{25}$$

The spatial polynomial basis matrix is defined as

$$\Phi(x) = \begin{bmatrix} 1 & 0 & 0 & 0 & \cdots & 0 \\ -1 & 2 & 0 & 0 & \cdots & 0 \\ 1 & -6 & 6 & 0 & \cdots & 0 \\ -1 & 12 & -30 & 20 & \ddots & 0 \\ \vdots & \vdots & \vdots & \vdots & \vdots & \vdots \end{bmatrix} \begin{bmatrix} 1 \\ x \\ x^2 \\ x^3 \\ x^4 \\ \vdots \end{bmatrix}, \tag{26}$$

Using the operational matrix approach, differentiation and integration with respect to x and t can be expressed in matrix form. The first derivative with respect to t is given by

$$\frac{\partial}{\partial t} y_{m,n}(x,t) = D^{(1)} \left(\Phi(x)^T\right) C \, \Upsilon(t) \tag{27}$$

where $D^{(1)}$ is the operational derivative matrix acting on the basis $\Upsilon(t)$. The second derivative with respect to x

$$\frac{\partial^2}{\partial x^2} y_{m,n}(x,t) = D^{(2)} \left(\Phi(x)^T\right) C \, \Upsilon(t) \tag{28}$$

where $D^{(2)}$ is the second-order operational derivative matrix associated with $\Phi(x)$, such that

$$D^{(2)} \, \Phi(x) = \begin{bmatrix} 0 & 0 & 0 & 0 & \cdots & 0 \\ 0 & 0 & 0 & 0 & \cdots & 0 \\ 12 & 0 & 0 & 0 & \cdots & 0 \\ -60 & 120 & 0 & 0 & \ddots & 0 \\ \vdots & \vdots & \vdots & \vdots & \vdots & \vdots \end{bmatrix} \begin{bmatrix} 1 \\ x \\ x^2 \\ x^3 \\ x^4 \\ \vdots \end{bmatrix}. \tag{29}$$

Remark. In Eqs. (27)–(29), $D^{(1)}$ and $D^{(2)}$ denote the first- and second-order *operational derivative matrices* associated with the shifted Legendre basis functions. For the shifted Legendre polynomial $\tilde{P}_i(x)$ on $[0,1]$, the derivative can be expressed as

$$\frac{d}{dx}\tilde{P}_i(x) = \sum_{k=0}^{i-1} d_{ik}^{(1)} \, \tilde{P}_k(x), \qquad \frac{d^2}{dx^2}\tilde{P}_i(x) = \sum_{k=0}^{i-2} d_{ik}^{(2)} \, \tilde{P}_k(x),$$

where $d_{ik}^{(1)}$ and $d_{ik}^{(2)}$ are the coefficients obtained from the recurrence relations of Legendre polynomials. Consequently, the operational matrices $D^{(1)} = [d_{ik}^{(1)}]_{(m+1)\times(m+1)}$ and $D^{(2)} = [d_{ik}^{(2)}]_{(m+1)\times(m+1)}$ satisfy

$$\frac{d}{dx}\Phi(x) = D^{(1)}\Phi(x), \qquad \frac{d^2}{dx^2}\Phi(x) = D^{(2)}\Phi(x),$$

where $\Phi(x) = [\tilde{P}_0(x), \tilde{P}_1(x), \ldots, \tilde{P}_m(x)]^T$. This general form holds for any polynomial of order m, while the explicit numerical example in Eq. (29) illustrates the case for small m.

The Atangana–Baleanu–Caputo (ABC) fractional derivative is approximated by:

$${}_0^{ABC}\mathrm{D}_x^{\alpha} y_{m,n}(x,t) = \Phi(x)^T \, C \, {}_0^{ABC}\mathrm{D}_t^{\alpha,\mu,\gamma} \Upsilon(t), \tag{30}$$

where

$${}_0^{ABC}\mathrm{D}_t^{\alpha} \Upsilon(t) = [{}_0^{ABC}\mathrm{D}_t^{\alpha} \tilde{P}_0(t), {}_0^{ABC}\mathrm{D}_t^{\alpha} \tilde{P}_1(t), \ldots, {}_0^{ABC}\mathrm{D}_t^{\alpha} \tilde{P}_n(t)], \tag{31}$$

which is explained in Theorem 1.

3.1. Approximation for the Time-Fractional Cattaneo Equation

We now apply the proposed method to solve the time-fractional Cattaneo equation

$$\frac{\partial}{\partial t}y(x,t) + {}_0^{ABC}\mathrm{D}_t^{\alpha} y(x,t) = \frac{\partial^2}{\partial x^2}y(x,t) + h(x,t), \quad 1 < \alpha < 2. \tag{32}$$

Substituting the spectral approximations yields the discrete form:

$$\Phi(x)^T C\ D^{(1)}\Upsilon(t) + \Phi(x)^T C\ {}_0^{ABC}\mathrm{D}_t^{\alpha,\mu,\gamma}\Upsilon(t) - D^{(2)}\Phi(x)^T C\ \Upsilon(t) - h(x,t) = 0, \quad 1 < \alpha < 2. \tag{33}$$

The initial conditions are given by:

$$y(x,0) = \Phi(x)^T C\ \Upsilon(0), \quad \frac{d}{dt}y(x,0) = \Phi(x)^T C\ D^{(1)}\Upsilon(0), \quad 0 \le x \le 1. \tag{34}$$

The boundary conditions are:

$$y(0,t) = \Phi(0)^T C\ \Upsilon(t), \quad y(1,t) = \Phi(1)^T C\ \Upsilon(t), \quad 0 < t < 1. \tag{35}$$

We discretize the spatial and temporal domains using Newton–Cotes nodes:

$$x_i = \frac{2i-1}{2(m+1)} \quad and \quad t_j = \frac{2j-1}{2n} \quad for \quad i = 1, \ldots, m-1 \quad and \quad j = 1, \ldots, n-1.$$

The discretized form of the time-fractional Cattaneo equation becomes:

$$\Phi(x_i)^T C\ D^{(1)}\Upsilon(t_j) + \Phi(x_i)^T C\ {}_0^{ABC}\mathrm{D}_t^{\alpha}\Upsilon(t_j) - D^{(2)}\Phi(x_i)^T C\ \Upsilon(t_j) - h(xi,t_j) = 0, \quad 1 < \alpha < 2. \tag{36}$$

Initial and boundary conditions are enforced at the corresponding nodes as

$$y(x_i,0) = \Phi(x_i)^T C\ \Upsilon(0), \quad \frac{d}{dt}y(x_i,0) = \Phi(x_i)^T C\ D^{(1)}\Upsilon(0), \tag{37}$$

and

$$y(0,t_j) = \Phi(0)^T C\ \Upsilon(t_j), \quad y(1,t_j) = \Phi(1)^T C\ \Upsilon(t_j). \tag{38}$$

By enforcing the residual equation at all interior nodes, where $i = 1, \ldots, m-1$ and $j = 1, \ldots, n-1$, we obtain $(m-1)(n-1)$ algebraic equations. Including the initial and boundary conditions at the appropriate points adds further constraints. In total, we obtain a system of $(m+1)(n+1)$ equations, which can be solved to determine the unknown coefficients c_{ij} for $i = 0, \ldots, m$ and $j = 0, \ldots, n$.

Remark. Newton–Cotes nodes are used for simplicity and because they include the endpoints, making it easier to impose boundary and initial conditions. Although Gauss–Legendre nodes give slightly higher accuracy, the Newton–Cotes choice offers straightforward implementation and still achieves spectral convergence.

4. Convergence Analysis

In this section, we prove the convergence of our approximate solution obtained by the shifted Legendre spectral method for the time-fractional PDE with the Atangana–Baleanu–Caputo (ABC) derivative of order $\alpha \in (1, 2)$.

Theorem 2. *Let $u(x, t)$ be the exact solution of the time-fractional PDE*

$$ {}_0^{ABC}D_t^{\alpha} u(x,t) = \mathcal{L}u(x,t) + f(x,t), \quad \alpha \in (1,2), $$

where $\mathcal{L}$ is a spatial differential operator with sufficiently smooth coefficients, and f is smooth on the considered domain. Let $u_N(x, t)$ be the approximate solution obtained by the shifted Legendre spectral method using N basis functions in space. If $u(\cdot, t) \in H^m(\Omega)$ for $m > 0$ and for all $t \in [0, T]$, then the following error estimate holds:

$$ \|u(\cdot,t) - u_N(\cdot,t)\|_{L^2(\Omega)} \leq CN^{-m} \|u(\cdot,t)\|_{H^m(\Omega)}, $$

for some constant $C > 0$ independent of N and t. Consequently, $u_N \to u$ in $L^2(\Omega)$ as $N \to \infty$.

Proof. The shifted Legendre spectral approximation projects $u(\cdot, t)$ onto the polynomial space P_N of degree at most N. Let P_N denote the $L^2(\Omega)$ projection operator. Then

$$ u_N(\cdot,t) = P_N u(\cdot,t) + (\text{discretization error from time derivative}). $$

From the standard spectral approximation theory [29], for $u(\cdot, t) \in H^m(\Omega)$ we have

$$ \|u(\cdot,t) - P_N u(\cdot,t)\|_{L^2(\Omega)} \leq CN^{-m} \|u(\cdot,t)\|_{H^m(\Omega)}. $$

The ABC fractional derivative of order $\alpha \in (1, 2)$ does not affect the spatial approximation order, since the temporal discretization is handled separately and the spatial operator $\mathcal{L}$ acts only in x. The stability of the scheme ensures that the temporal error does not amplify the spatial projection error. Thus, the total error satisfies

$$ \|u(\cdot,t) - u_N(\cdot,t)\|_{L^2(\Omega)} \leq CN^{-m} \|u(\cdot,t)\|_{H^m(\Omega)}. $$

Since $m > 0$, we conclude that $u_N \to u$ in $L^2(\Omega)$ as $N \to \infty$.

Remark. The convergence result is extended to include both spatial and temporal discretizations. For the approximate solution $u_{m,n}(x, t)$, we have

$$ \|u - u_{m,n}\|_{L^2(\Omega \times [0,T])} \leq C\,(m^{-p} + n^{-q}), $$

where $p, q > 0$ depend on the smoothness of $u(x, t)$. This establishes the full space–time convergence of the proposed spectral method.

5. Numerical Results and Discussion

In this section, we apply the proposed method—based on the two-dimensional expansion of shifted Legendre polynomials as defined in Equation (23), and incorporating the Atangana–Baleanu–Caputo (ABC) fractional derivative introduced in Definition (4) to three illustrative examples of the time-fractional Cattaneo equation.

Dirichlet boundary conditions are imposed to represent fixed temperatures at both ends of the medium, which correspond to a rod or slab in contact with thermal reservoirs of constant temperature. This setup is physically meaningful in heat and diffusion transport, as it models systems with controlled boundaries where the heat flux or concentration evolves internally while the boundary values remain constant. Such conditions allow clear observation of the finite-speed propagation and memory effects described by the time-fractional Cattaneo equation.

Example 1. *The time-fractional Cattaneo equation represents a fundamental extension of the classical heat conduction law, incorporating memory effects and nonlocal behavior through fractional derivatives. Unlike the traditional Fourier model, it captures finite propagation speed of thermal signals and accounts for anomalous diffusion phenomena observed in complex media. Such features make it a powerful tool for modeling heat transfer in biological tissues, heterogeneous materials, and advanced engineering systems. Consider the time fractional Cattaneo equation*

$$\frac{\partial}{\partial t}y(x,t) + {}_0^{ABC}\mathrm{D}_t^{\alpha}y(x,t) = \frac{\partial^2}{\partial x^2}y(x,t) + h(x,t), 1 < \alpha \leq 2,\ \mu > 0 \quad and \quad \gamma \in N. \quad (39)$$

We assume the following initial conditions:

$$y(x,0) = 0, \quad \frac{\partial y}{\partial t}(x,0) = \sin(x), \quad 0 \leq x \leq 1.$$

The boundary conditions are taken as:

$$y(0,t) = 0, \quad y(1,t) = t\sin(1), \quad t > 0.$$

where $h(x,t) = (1+t)\sin(x)$, and the analytic solution is $y(x,t) = t\sin(x)$. For applying the proposed method we have equation (39) in this form:

$$C^T\Phi(x)\Upsilon'(t) + C^T\Phi(x){}_0^{ABC}\mathrm{D}_t^{\alpha}\Upsilon(t) = C^T\Phi''(x)\Upsilon(t) + h(x,t), \quad 1 < \alpha \leq 2 \quad (40)$$

The initial and boundary conditions respectively are:

$$C^T\Phi(x)\Upsilon(0) = 0, \quad C^T\Phi(x)\Upsilon'(0) = sin(x), \quad 0 \leq x \leq 1$$

and

$$C^T\Phi(0)\Upsilon(t) = 0, \quad C^T\Phi(1)\Upsilon(t) = t\sin(1), \quad t > 0.$$

We now apply the Newton–Cotes points to Equation (40), as well as to the initial and boundary conditions. This yields a system of equations, which can be solved to obtain the coefficients c_{ij} for $i = 0, ..., m$ and $j = 0, ..., n$. Substituting these coefficients into Equation (23) provides the approximate solution.
In Figure 1, we plot the approximate solution of Example 1 with different values of α confirming that the solution maintains its form across the fractional orders considered. In Table 1, we show the absolute error between the approximate solution and analytic

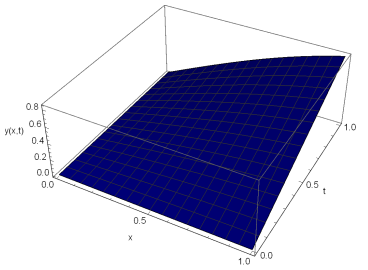

(a) The approximate solution for $m = n = 10$. with $\alpha \to 2$.

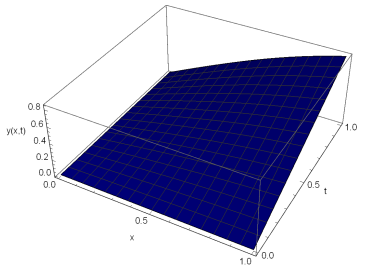

(b) The approximate solution for n=m=10 with $\alpha = 1.9$.

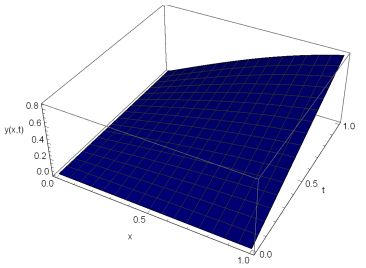

(c) The approximate solution for n=m=10 with $\alpha = 1.5$.

Figure 1: Graph of 3D approximate solutions $y(x, t)$ of Example 1 at different values of fractional order α and $\mu = \gamma = 1$.

solution at different values of m and n. In Figure 2, we plot the absolute error between the approximate solution and analytic solution for different values of α at different values of t.

The graphical representations and numerical tables clearly demonstrate the effectiveness of the proposed method. The plots illustrate that the numerical solutions closely follow the exact solution across the entire domain, confirming the accuracy and stability of the scheme. The error curves remain uniformly small, indicating the robustness of the approach even for varying parameters. Furthermore, the tables of absolute errors highlight the excellent convergence behavior of the method, with errors decreasing consistently as the discretization is refined. These results collectively verify that the proposed scheme provides both reliable and highly accurate approximations for the time-fractional Cattaneo equation.

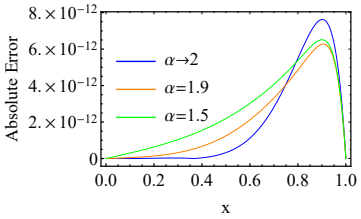

(a) The absolute error between the analytic solution and approximate solution for $n = m = 10$ with $t = 0.5$.

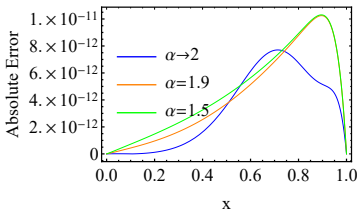

(b) The absolute error between the analytic solution and approximate solution for $n = m = 10$ with $t = 0.75$.

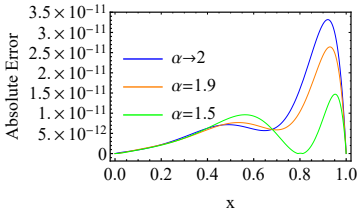

(c) The absolute error between the analytic solution and approximate solution for $n = m = 10$ with $t = 1$.

Figure 2: Graph of the absolute error between analytic solution and approximate solution of Example 2 for $n = m = 10$ and $\mu = \gamma = 1$ with different values of t.

Table 1: The Absolute Error Between the Approximate Solution and the Analytic Solution for Example 1 with $\alpha = 1.7$ and $\mu = \gamma = 1$.

x_i	t	The Error for $n = m = 8$	The Error for $n = m = 9$	The Error for $n = m = 10$
0.2	0.5	$2.99427 * 10^{-10}$	$6.15387 * 10^{-12}$	$4.71262 * 10^{-13}$
0.5		$1.19721 * 10^{-9}$	$2.46842 * 10^{-11}$	$1.88918 * 10^{-12}$
0.75		$2.82641 * 10^{-9}$	$5.82703 * 10^{-11}$	$4.45532 * 10^{-12}$
1		$1.11022 * 10^{-16}$	$2.55351 * 10^{-15}$	$5.55112 * 10^{-17}$
0.2	0.75	$8.50549 * 10^{-10}$	$1.74812 * 10^{-11}$	$1.3391 * 10^{-12}$
0.5		$2.62241 * 10^{-9}$	$5.4131 * 10^{-11}$	$4.1443 * 10^{-12}$
0.75		$5.00014 * 10^{-9}$	$1.03087 * 10^{-10}$	$7.8747 * 10^{-12}$
1		$3.34288 * 10^{-13}$	$3.77476 * 10^{-15}$	$3.33067 * 10^{-16}$
0.2	1	$1.27228 * 10^{-9}$	$3.66888 * 10^{-11}$	$2.02982 * 10^{-12}$
0.5		$5.24942 * 10^{-9}$	$6.56428 * 10^{-11}$	$8.02669 * 10^{-12}$
0.75		$5.76675 * 10^{-9}$	$1.80569 * 10^{-10}$	$9.47165 * 10^{-12}$
1		$3.89955 * 10^{-12}$	$4.80727 * 10^{-14}$	$6.66134 * 10^{-16}$

Example 2. *In the second example, we investigate the same time-fractional Cattaneo equation as in (39), but under a different source term $h(x,t)$ together with new initial and boundary conditions. This allows us to test the flexibility of the proposed method*

in handling varied problem settings and to further confirm its accuracy and reliability. Consider the time fractional Cattaneo equation (39).

We assume the following initial conditions:

$$y(x,0)=0, \quad \frac{\partial y}{\partial t}(x,0)=(1-x)\cos(x), \quad 0\le x\le 1.$$

The boundary conditions are taken as:

$$y(0,t)=t, \quad y(1,t)=0, \quad t>0.$$

where $h(x,t)=(1+t)(1-x)\cos(x)-2t\sin(x)$ and the analytic solution is $t(1-x)\cos(x)$. For applying the proposed method we have equation (39) in this form:

$$C^T\Phi(x)\Upsilon'(t)+C^T\Phi(x){}_0^{ABC}\mathrm{D}_t^{\alpha}\Upsilon(t)=C^T\Phi''(x)\Upsilon(t)+h(x,t), \quad 1<\alpha\le 2 \tag{41}$$

The initial and boundary conditions respectively are:

$$C^T\Phi(x)\Upsilon(0)=0, \quad C^T\Phi(x)\Upsilon'(0)=(1-x)\cos(x), \quad 0\le x\le 1$$

and

$$C^T\Phi(0)\Upsilon(t)=t, \quad C^T\Phi(1)\Upsilon(t)=0, \quad t>0.$$

We now apply the Newton–Cotes points to Equation (41), as well as to the initial and boundary conditions. This yields a system of equations, which can be solved to obtain the coefficients c_{ij} for $i=0,...,m$ and $j=0,...,n$. Substituting these coefficients into Equation (23) provides the approximate solution. In Figure 3, we compare the approximate solutions of Example 2 with $m=n=10$ for different values of α confirming that the solution maintains its form across the fractional orders considered. In Figure 4, we plot the absolute error between the analytic and approximate solution of Example 2 with different values of α at different values of t.

In Table 2, we show the absolute error between the approximate solution and analytic solution for different values of m and n.

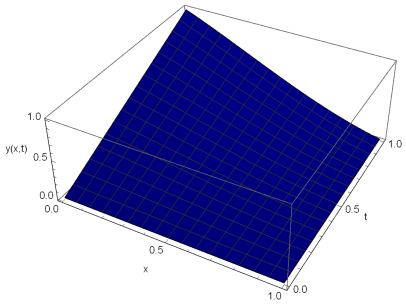

(a) The approximate solution with $n = m = 10$ for $\alpha = 1.9$.

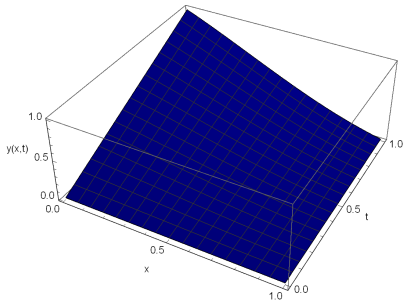

(b) The approximate solution with $n = m = 10$ for $\alpha = 1.7$.

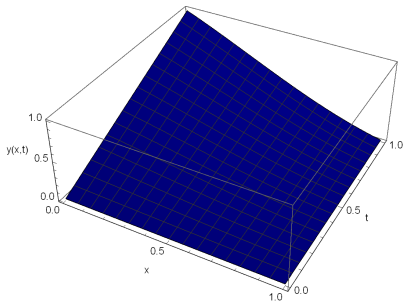

(c) The approximate solution with $n = m = 10$ for $\alpha = 1.5$.

Figure 3: Graph of 3D approximate solutions $y(x,t)$ of Example 2 for different fractional orders α and $\mu = \gamma = 1$.

Table 2: The Absolute Error Between the Approximate Solution and the Analytic Solution for Example 2 with $\alpha \to 2$ and $\mu = \gamma = 1$.

x_i	t	The Error for $n = m = 8$	The Error for $n = m = 9$	The Error for $n = m = 10$
0.2	0.5	$1.1826 * 10^{-10}$	$7.48124 * 10^{-13}$	$2.93043 * 10^{-13}$
0.5		$3.72807 * 10^{-9}$	$6.76754 * 10^{-11}$	$7.54966 * 10^{-12}$
0.75		$4.79501 * 10^{-8}$	$9.82067 * 10^{-10}$	$1.29042 * 10^{-10}$
1		$3.76952 * 10^{-18}$	$2.02171 * 10^{-14}$	$1.4904 * 10^{-17}$
0.2	0.75	$1.46942 * 10^{-9}$	$3.11556 * 10^{-11}$	$2.40996 * 10^{-12}$
0.5		$4.27502 * 10^{-8}$	$8.7062 * 10^{-10}$	$1.14236 * 10^{-10}$
0.75		$1.38917 * 10^{-7}$	$2.7897 * 10^{-9}$	$2.70234 * 10^{-10}$
1		$3.08669 * 10^{-12}$	$3.17882 * 10^{-14}$	$1.18969 * 10^{-15}$
0.2	1	$2.58444 * 10^{-8}$	$5.04681 * 10^{-10}$	$6.69726 * 10^{-11}$
0.5		$1.22147 * 10^{-7}$	$2.49645 * 10^{-9}$	$2.48266 * 10^{-10}$
0.75		$1.45674 * 10^{-7}$	$1.43257 * 10^{-9}$	$1.18856 * 10^{-10}$
1		$3.60443 * 10^{-11}$	$4.1316 * 10^{-13}$	$3.4733 * 10^{-14}$

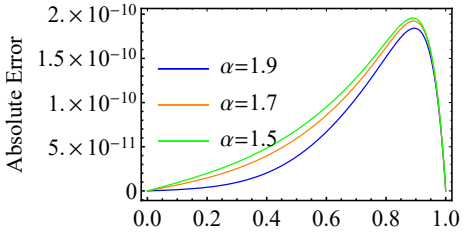

(a) The absolute error between the analytic solution and approximate solution for $n = m = 10$ with $t = 0.5$.

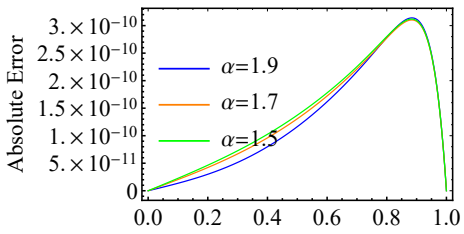

(b) The absolute error between the analytic solution and approximate solution for $n = m = 10$ with $t = 0.75$.

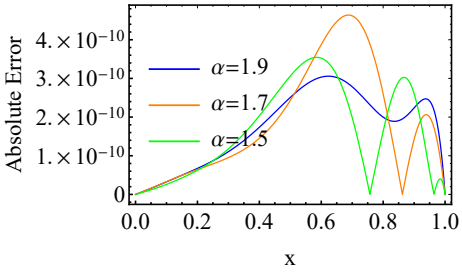

(c) The absolute error between the analytic solution and approximate solution for $n = m = 10$ with $t = 1$.

Figure 4: Graph of the absolute error between analytic solution and approximate solution of Example 2 for $n = m = 10$ and $\mu = \gamma = 1$ with different values of t.

Example 3. *In the third example, we again consider the time-fractional Cattaneo equation as formulated in equation (39), but with a distinct source term $h(x,t)$ and a new configuration of initial and boundary conditions. This example is designed to demonstrate the robustness and adaptability of the proposed numerical approach in handling more complex spatial behaviors and variable source dynamics. The case also provides an opportunity to validate the accuracy of the method against a known analytical solution.This example verifies the consistency of the proposed algorithm when applied to problems with polynomial-type exact solutions and nontrivial source terms, highlighting its capability to preserve spatial accuracy and temporal convergence. Consider the time fractional Cattaneo equation*

$$\frac{\partial}{\partial t}y(x,t) + {}_0^{ABC}\mathrm{D}_t^{\alpha} y(x,t) = \frac{\partial^2}{\partial x^2}y(x,t) + h(x,t), \tag{42}$$

for

$$1 < \alpha \leq 2,\ \mu > 0 \quad \textit{and} \quad \gamma \in N.$$

We assume the following initial conditions:

$$y(x,0) = 0, \quad \frac{\partial y}{\partial t}(x,0) = 0, \quad x > 0.$$

The boundary conditions are taken as:

$$y(0,t) = 0, \quad y(1,t) = 0, \quad t > 0.$$

where

$$h(x,t) = 2(1-x^2)x^{16/3}t + \frac{\Gamma[3]}{1-\alpha_1}E^{\gamma}_{\alpha_1,\mu+1}(\lambda,t) + t^2(\frac{418}{9}x^{16/3} - \frac{208}{9}x^{10/3})$$

and the analytic solution is $y(x,t) = t^2(1-x^2)x^{16/3}$.

For applying the proposed method we have equation (39) in this form:

$$C^T\Phi(x)\Upsilon'(t) + C^T\Phi(x){}^{ABC}_{0}\mathrm{D}^{\alpha}_{t}\Upsilon(t) = C^T\Phi''(x)\Upsilon(t) + h(x,t), \quad 1 < \alpha \leq 2 \tag{43}$$

The initial and boundary conditions respectively are:

$$C^T\Phi(x)\Upsilon(0) = 0, \quad C^T\Phi(x)\Upsilon'(0) = 0, \quad x > 0$$

and

$$C^T\Phi(0)\Upsilon(t) = 0, \quad C^T\Phi(1)\Upsilon(t) = 0, \quad t > 0.$$

We now apply the Newton–Cotes points to Equation (43), as well as to the initial and boundary conditions. This yields a system of equations, which can be solved to obtain the coefficients c_{ij} for $i = 0, ..., m$ and $j = 0, ..., n$. Substituting these coefficients into Equation (23) provides the approximate solution. In Figure 5, we plot the approximate solutions of Example 3 with different values of α confirming that the solution maintains its form across the fractional orders considered. In Figure 6, we plot the absolute error between the analytic and approximate solutions of Example 3 with $\alpha \to 2$.

In Figure 7, we plot the absolute error between the approximate solution and analytic solution at various values of t. In Figure 8, we show the absolute error for different values of α in each case we differ the value of t. In Figure 9, we plot the absolute ABC fractional derivative of the approximate solution fot the previous examples at various time. In Table 3, we show the absolute error between the approximate solution and analytic solution for different values of m and n.

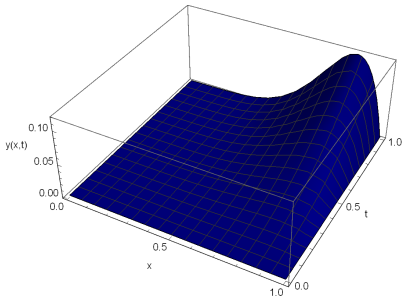

(a) The approximate solution with $n = m = 10$ for $\alpha = 1.9$.

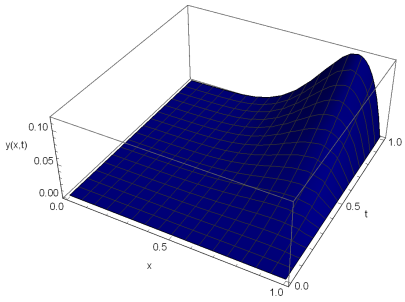

(b) The approximate solution with $n = m = 10$ for $\alpha = 1.7$.

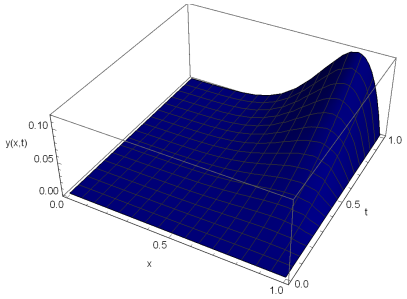

(c) The approximate solution with $n = m = 10$ for $\alpha = 1.5$.

Figure 5: Graph of 3D approximate solutions $y(x,t)$ of Example 3 at multiple α values and $\mu = \gamma = 1$.

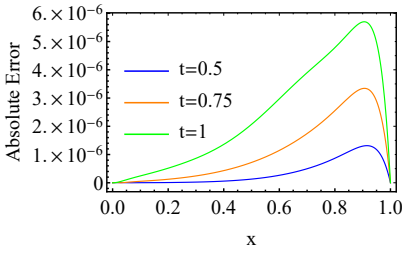

(a) The absolute error between the analytic solution and approximate solution for $n = m = 10$ with $\alpha = 1.9$.

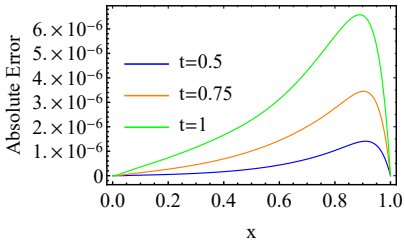

(b) The absolute error between the analytic solution and approximate solution for $n = m = 10$ with $\alpha = 1.7$.

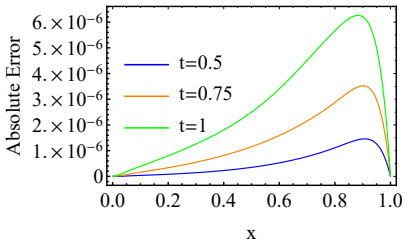

(c) The absolute error between the analytic solution and approximate solution for $n = m = 10$ with $\alpha = 1.5$.

Figure 7: Graph of the absolute error between the analytic and approximate solutions of Example 3, for $n = m = 10$, under different values of α and t with $\mu = \gamma = 1$.

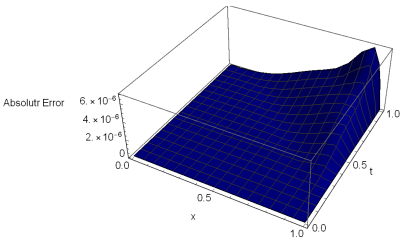

(a) The approximate solution with $n = m = 10$ for $\alpha \to 2$.

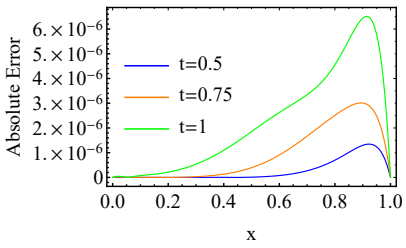

(b) The absolute error between analytic and approximate solutions with $n = m = 10$ for $\alpha \to 2$.

Figure 6: Graph the absolute error of Example 3 for $n = m = 10$ in 2D and in 3D with $\alpha \to 2$ and $\mu = \gamma = 1$.

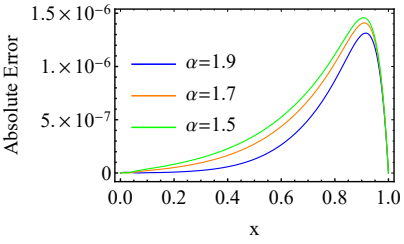

(a) The absolute error between the analytic solution and approximate solution for $n = m = 10$ at $t = 0.5$.

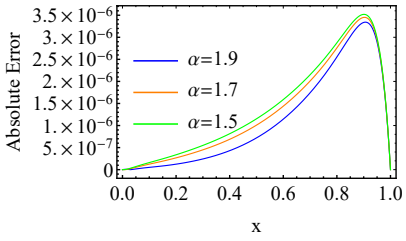

(b) The absolute error between the analytic solution and approximate solution for $n = m = 10$ at $t = 0.75$.

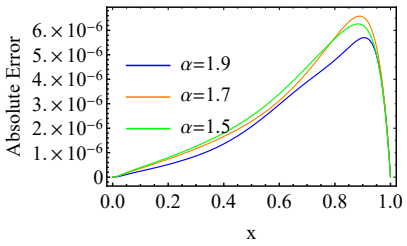

(c) The absolute error between the analytic solution and approximate solution for $n = m = 10$ at $t = 1$.

Figure 8: Graph of the absolute error between analytic solution and approximate solution of Example 3 for $n = m = 10$ with different values of α, $\mu = \gamma = 1$ and fixed value of t in each case.

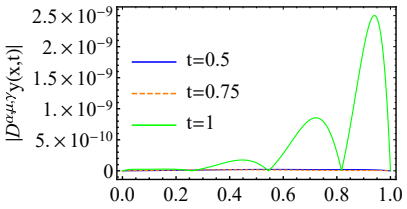

(a) The absolute ABC fractional derivative for Example 1 at $\alpha = 1.9$.

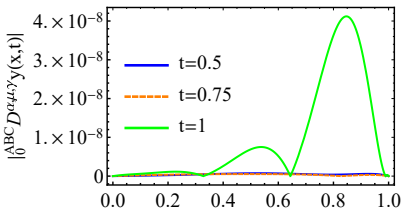

(b) The absolute ABC fractional derivative for Example 2 at $\alpha = 1.9$.

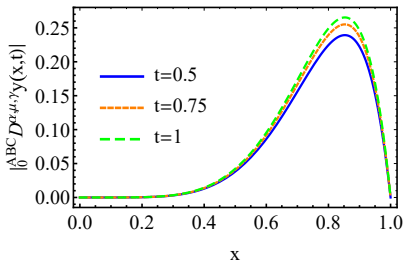

(c) The absolute ABC fractional derivative for Example 3 at $\alpha = 1.9$.

Figure 9: Graph of the absolute ABC fractional derivative with $\alpha = 1.9$ and $\mu = \gamma = 1$ at various time for all previous Examples.

Table 3: The Absolute Error Between the Approximate Solution and the Analytic Solution for Example 3 with $\alpha = 1.9$ and $\mu = \gamma = 1$.

x_i	t	The Error for $n = m = 8$	The Error for $n = m = 9$	The Error for $n = m = 10$
0.2	0.5	$5.04861 * 10^{-8}$	$1.12301 * 10^{-8}$	$8.31537 * 10^{-9}$
0.5		$6.70551 * 10^{-7}$	$1.48617 * 10^{-7}$	$1.29698 * 10^{-7}$
0.75		$3.48628 * 10^{-6}$	$7.65891 * 10^{-7}$	$6.61929 * 10^{-7}$
1		$3.79363 * 10^{-18}$	$2.59003 * 10^{-18}$	$1.07461 * 10^{-18}$
0.2	0.75	$6.65688 * 10^{-7}$	$1.47572 * 10^{-7}$	$1.24293 * 10^{-7}$
0.5		$3.8094 * 10^{-6}$	$8.29879 * 10^{-7}$	$7.19218 * 10^{-7}$
0.75		$1.12487 * 10^{-5}$	$2.43645 * 10^{-6}$	$2.11753 * 10^{-6}$
1		$1.42785 * 10^{-17}$	$1.11675 * 10^{-19}$	$8.18061 * 10^{-18}$
0.2	1	$2.78842 * 10^{-6}$	$6.30815 * 10^{-7}$	$5.1629 * 10^{-7}$
0.5		$1.0846 * 10^{-5}$	$2.23758 * 10^{-6}$	$2.06741 * 10^{-6}$
0.75		$2.32872 * 10^{-5}$	$5.3756 * 10^{-6}$	$4.33013 * 10^{-6}$
1		$1.2163 * 10^{-16}$	$4.76285 * 10^{-17}$	$2.36227 * 10^{-16}$

Compared with FEM, FDM, and meshless methods [30–32], the proposed spectral collocation achieves faster (exponential) convergence with fewer grid points and simpler

implementation. Also it is to be noted that the method scales as $O((mn)^2)$ in time and $O(mn)$ in memory. For $m = n = 10$, runtime is under 0.3 s, showing high efficiency.

6. Conclusions

In this work, we developed a novel spectral collocation method for solving the time-fractional Cattaneo equation involving the ABC fractional derivative. By employing two-dimensional expansions of shifted Legendre polynomials and Newton–Cotes nodes for discretization, the proposed formulation transformed the original fractional partial differential equation into a tractable system of algebraic equations.

The main novelty of this study lies in integrating the (ABC) fractional operator with a generalized Mittag–Leffler kernel into a Legendre spectral–collocation framework, enabling high-accuracy solutions for fractional diffusion problems with non-singular memory effects.

The numerical results confirm that the Legendre spectral method achieves excellent accuracy and stability, producing errors significantly smaller than those obtained by existing approaches [2, 17]. The method demonstrated strong agreement with available analytical solutions which were explained in previous three examples, establishing its reliability and efficiency for modeling diffusion processes with memory effects.

For Example 1, Figure 1 presents the three-dimensional approximate solutions for different values of α, while Figure 2 illustrates the corresponding absolute errors at various time levels for the case $m = n = 10$ where the error within 10^{-12}. As reported in Table 1, increasing the value of m yields a clear reduction in the absolute error at $\alpha = 1.7$, confirming that higher polynomial degrees enhance the accuracy of the proposed method. For Example 2, Figure 3 displays the three-dimensional approximate solutions for different values of α with $m = n = 10$. The associated absolute errors are shown in Figure 4 at various time levels. It is observed that the error increases as t grows larger, while smaller values of t lead to lower errors where the error within 10^{-10}. Table 2 further reports the absolute error for values of α close to 2, providing additional evidence of the method's robustness. For Example 3, Figure 5 shows the approximate solution for different values of α, whereas Figure 6 illustrates the three-dimensional solution for α close to 2. The corresponding absolute errors are plotted in Figure 7 at different time levels, where it is evident that smaller values of t yield smaller errors. Figure 8 confirms that in all cases, the absolute error remains within the order of 10^{-6}. Finally, Table 3 demonstrates that for $\alpha = 1.9$, the absolute error consistently decreases with larger values of m and n, highlighting the effectiveness of the proposed spectral method. From the results of the previous examples, we conclude that the proposed method achieves errors less than half of those obtained by other existing approaches [2, 18]. The accuracy and convergence of the proposed Legendre spectral method were validated by comparison with spline-based and pseudospectral methods reported in the literature [2, 17–20]. The results exhibit consistent error trends and spectral convergence, confirming the reliability of the present approach. From a physical perspective, the model effectively captures finite-speed heat propagation and long-memory effects, which are essential in real-world applications such as nanoscale heat conduction, bioheat transfer, and phase-change thermal storage systems. The presented framework

can be extended to nonlinear fractional PDEs by coupling the spectral approximation with iterative solvers such as the Adomian decomposition or Newton–Raphson schemes. Furthermore, replacing the ABC kernel with generalized Mittag–Leffler or Prabhakar kernels requires only modifying the operational matrix of the fractional derivative, making the approach adaptable to a broad class of fractional models.

Beyond its application to the time–fractional Cattaneo diffusion model, the approach provides a flexible framework that can be extended to other classes of fractional differential equations involving non-singular kernels. For future work, we may focus on extending the method to multi–dimensional problems, variable-order derivatives, and nonlinear systems, as well as exploring its applicability in practical domains such as bioheat transfer, energy storage, and nanoscale heat transport.

Acknowledgements

The authors would like to thank Jordan University of Science and Technology (Deanship of Research) for providing support under project No. 20250372 to complete this research.

References

[1] A. A. Kilbas, H. M. Srivastava, and J. J. Trujillo. *Theory and Applications of Fractional Differential Equations*, volume 204. Elsevier, 2006.

[2] M. Yaseen, Q. U. N. Arif, R. George, and S. Khan. Comparative numerical study of spline-based numerical techniques for time-fractional cattaneo equation in the sense of caputo–fabrizio. *Fractal and Fractional*, 6(2):50, 2022.

[3] A. Atangana and D. Baleanu. New fractional derivatives with nonlocal and non-singular kernel: theory and application to heat transfer model, 2016. arXiv preprint.

[4] J. C. Zhou, S. Salahshour, A. Ahmadian, and N. Senu. Modeling the dynamics of covid-19 using fractal–fractional operator with a case study. *Results in Physics*, 33:105103, 2022.

[5] M. Wali, S. Arshad, S. M. Eldin, and I. Siddique. Numerical approximation of atangana–baleanu caputo derivative for space–time fractional diffusion equations. *AIMS Mathematics*, 8(7):15129–15147, 2023.

[6] M. Xu and J. Wang. Analytical solution of the time-fractional cattaneo heat equation for a finite slab under pulse heat flux. *Applied Mathematics and Mechanics*, 39(9):1267–1280, 2018.

[7] K. Wang, Y. Zhang, and H. Liu. Analysis of a time–space fractional bioheat transfer model for laser irradiation. *International Journal of Heat and Mass Transfer*, 176:121422, 2021.

[8] A. Chen and L. Nong. Efficient galerkin finite element methods for a time-fractional cattaneo equation. *Advances in Difference Equations*, 2020(1):545, 2020.

[9] L. Mohan and A. Prakash. Stability and numerical analysis of the generalised time-

fractional cattaneo model for heat conduction in porous media. *European Physical Journal Plus*, 138(3):294, 2023.

[10] M. Yaseen, Q. U. N. Arif, R. George, and S. Khan. Comparative numerical study of spline-based numerical techniques for time-fractional cattaneo equation in the sense of caputo–fabrizio. *Fractal and Fractional*, 6:50, 2022.

[11] W. Xu, J. Ba, J. Cao, and C. Luo. Adaptive-coefficient finite difference frequency domain method for solving time-fractional cattaneo equation with absorbing boundary condition. *Fractal and Fractional*, 8(3):146, 2024.

[12] S. Kumar and P. Pandey. A legendre spectral finite difference method for the solution of non-linear space–time fractional burger's–huxley and reaction–diffusion equation with atangana–baleanu derivative. *Chaos, Solitons & Fractals*, 130:109402, 2020.

[13] X. Xu and F. Zhou. Orthonormal euler wavelets method for time-fractional cattaneo equation with caputo–fabrizio derivative. *AIMS Mathematics*, 8(2):2736–2762, 2023.

[14] D. Baleanu, B. Shiri, H. M. Srivastava, and M. Al Qurashi. A chebyshev spectral method based on operational matrix for fractional differential equations involving non-singular mittag-leffler kernel. *Advances in Difference Equations*, 2018(1):1–23, 2018.

[15] M. Basima, N. Senua, A. Ahmadian, Z. B. Ibrahim, and S. Salahshour. Solving fractional variable-order differential equations of the non-singular derivative using jacobi operational matrix. *Journal of the Nigerian Society of Physical Sciences*, 5(1):101–112, 2023.

[16] Y. Zhang and X. Feng. Uniqueness of identifying multiple parameters in a time-fractional cattaneo equation. *Applied Mathematics Letters*, 163:109438, 2025.

[17] F. A. Shah, W. Boulila, A. Koubaa, and N. Mlaiki. Numerical solution of advection–diffusion equation of fractional order using chebyshev collocation method. *Fractal and Fractional*, 7(10):762, 2023.

[18] F. A. Shah and T. Abdeljawad. Numerical modelling of advection–diffusion equation using chebyshev spectral collocation method and laplace transform. *Results in Applied Mathematics*, 21:100420, 2024.

[19] F. A. Shah, D. Santina, N. Mlaiki, and S. Aljawi. Application of a hybrid pseudospectral method to a new two-dimensional multi-term mixed sub-diffusion and wave-diffusion equation of fractional order. *Networks and Heterogeneous Media*, 19(1):44–85, 2024.

[20] F. A. Shah, S. Aljawi, S. Bouzgarrou, and F. M. Alotaibi. Efficient computational hybrid method for the solution of 2d multi-term fractional order advection–diffusion equation. *Physica Scripta*, 99(6):065272, 2024.

[21] M. Alesemi. Numerical analysis of fractional-order parabolic equation involving atangana–baleanu derivative. *Symmetry*, 15:237, 2023.

[22] M. Hijazi, M. S. Ajeel, K. Al-Khaled, and H. Al-Khalid. Perturbation methods for solving non-linear ordinary differential equations. *IAENG International Journal of Applied Mathematics*, 54(10):2070–2082, 2024.

[23] Jian-Cun Zhou, Soheil Salahshour, Ali Ahmadian, and Norazak Senu. Modeling the dynamics of covid-19 using fractal–fractional operator with a case study. *Results in*

Physics, 33:105103, 2022.

[24] K. Mamehrashi and F. Soltanian. A numerical technique for solving a class of 2d variational problems using legendre spectral method. *Computational Methods for Differential Equations*, 6(4):471–482, 2018.

[25] A. H. Bhrawy, E. H. Doha, S. S. Ezz-Eldien, and M. A. Abdelkawy. A numerical technique based on the shifted legendre polynomials for solving the time-fractional coupled kdv equations. *Calcolo*, 53(1):1–17, 2016.

[26] V. K. Patel, S. Singh, and V. K. Singh. Two-dimensional shifted legendre polynomial collocation method for electromagnetic waves in dielectric media via almost operational matrices. *Mathematical Methods in the Applied Sciences*, 40(10):3698–3717, 2017.

[27] T. Abdeljawad and D. Baleanu. On fractional derivatives with generalized mittag-leffler kernels. *Advances in Difference Equations*, 2018(1):1–15, 2018.

[28] A. A. Almalki and S. Tamimi. A computational method for fractional equations using legendre polynomials and mittag-leffler kernels. *Journal of King Saud University–Science*, 37, 2025.

[29] C. Canuto, M. Y. Hussaini, A. Quarteroni, and T. A. Zang. *Spectral Methods: Fundamentals in Single Domains*. Springer-Verlag, Berlin, 2006.

[30] A. Chen and L. Nong. Efficient galerkin finite element methods for a time-fractional cattaneo equation. *Advances in Difference Equations*, 2020:545, 2020.

[31] L. Mohan and A. Prakash. Stability and numerical analysis of the generalised time-fractional cattaneo model for heat conduction in porous media. *European Physical Journal Plus*, 138:294, 2023.

[32] Mubashara Wali, Sadia Arshad, Sayed M. Eldin, and Imran Siddique. Numerical approximation of atangana–baleanu caputo derivative for space–time fractional diffusion equations. *AIMS Mathematics*, 8(7):15129–15147, 2023.